further work is necessary. Moreover, the neglect of folded-back chain configurations could mean that larger differences in the effective length $\langle L \rangle$ could exist than predicted by eq 3, so that further interpretation may require a more elaborate statistical mechanical analysis.

Finally, the isobaric coefficient of thermal expansion $\alpha \equiv (\langle L \rangle^{-1} \partial \langle L \rangle / \partial T)_P$ can be estimated from the temperature dependence of the ^{2}H NMR quadrupolar splittings[32] of the per-^{2}H-16:0 chains of the two bilayers using eq 3. An average value of $\alpha \simeq -1.5 \times 10^{-3}$ K^{-1} is obtained in both cases, consistent with previous X-ray[77,82] and ^{2}H NMR studies[32,72] of various phospholipid bilayers in the L_α phase.

5. Conclusions and Biological Significance

To summarize, we have discovered significant differences in conformation-dependent properties of the acyl chains of polyunsaturated and saturated phospholipid bilayers using ^{2}H NMR. The results lend themselves to a simplified statistical mechanical interpretation, and may eventually contribute to a better understanding of the biological roles of polyunsaturated phospholipids in membranes. Qualitatively, the behavior of the saturated chains of bilayers composed of asymmetric, saturated–polyunsaturated phosphatidylcholines appears to reflect an increase in their configurational freedom relative to symmetric, disaturated phospholipids. Thus, the lateral chain packing in polyunsaturated phospholipid bilayers may be significantly different from that in bilayers composed of phospholipids with two saturated acyl chains. The increased chain configurational freedom can be explained in terms of an increase in the equilibrium area at which attractive and repulsive forces acting upon the chains are balanced. This in turn could have implications for the energetics of functionally linked, membrane protein conformational changes. For example, given that an intrinsic membrane protein increases its cross-sectional area $A^{(p)}$ in undergoing a conformational change, the relative free energies of the initial and final states could include a contribution from the work of expansion against the lateral chain pressure π_c, given by

$$W = \int \pi_c \mathrm{d}A^{(p)} \cong 2\pi_c \Delta A^{(p)} \quad (4)$$

where the factor of two accounts for the apposed monolayers of the lipid bilayer. The above may provide one means by which lipid–protein interactions are coupled to specific biological membrane functions; other contributions may also be important and further experimental and theoretical investigations are necessary.

Acknowledgment. Thanks are due to Ken Dill, Thomas McIntosh, Jean-Paul Meraldi, Joachim Seelig, and Wilma Olson for their helpful criticisms of the manuscript. We are also grateful to Jeffrey Ellena and William Shoup for valuable assistance and to Edward Sternin and Myer Bloom for a listing of their de-Pakeing program. This research was funded by Grant EY03754 from the U.S. National Institutes of Health, and by the Thomas F. Jeffress and Kate Miller Jeffress Memorial Trust. A.S. was supported by a National Science Foundation predoctoral fellowship and J.M.B. by National Institutes of Health Postdoctoral Fellowship EY05746. M.F.B. is the recipient of Research Career Development Award EY00255 from the National Eye Institute.

(82) Rand, R. P.; Pangborn, W. A. *Biochim. Biophys. Acta* **1973**, *318*, 299–305.

Multifrequency Electron Spin Resonance of Molybdenum(V) and Tungsten(V) Compounds

Graeme R. Hanson,*[1a,c] Graham L. Wilson,[1a] Trevor D. Bailey,[1a,d] John R. Pilbrow,*[1b] and Anthony G. Wedd*[1a]

Contribution from the Department of Chemistry, La Trobe University, Bundoora, Victoria 3083, Australia, and the Department of Physics, Monash University, Clayton, Victoria 3168, Australia.
Received August 12, 1986

Abstract: The ESR spectra of a selection of molybdenum(V) and tungsten(V) compounds have been examined as a function of microwave frequency. In particular, reduced line widths at lower (S band: 2–4 GHz) microwave frequencies allow detection of ^{14}N, ^{1}H, ^{17}O, ^{77}Se, and ^{35,37}Cl superhyperfine interactions in certain of the following complexes: $[Mo(abt)_3]^-$ ($abtH_2$ = *o*-aminobenzenethiol), $[MO(XPh)_4]^-$ (M = Mo, W; X = S, Se), and *cis*-$[MoO(qtl)_2X]$ (X = Cl, Br; qtlH = quinoline-8-thiol). The redistribution of spectral information as a function of frequency, together with computer simulation, has allowed the determination of the hyperfine matrix and its relative orientation to the **g** matrix, in most cases. A d_{z^2}-based ground state is assigned to $[Mo(abt)_3]^-$ in contrast to d_{xy}-based ground states for the oxo-molybdenum(V) complexes. Axially symmetric sites are present in $[MO(XPh)_4]^-$ and monoclinic (C_s) sites in *trans*-$[MoOL(DMF)]^+$ (L = salen, salophen). The results provide strong motivation for a wider examination of transition metal species at lower microwave frequencies.

Recent advances in technology,[2–6] and the development of the loop-gap resonator in particular, have permitted more convenient measurement of electron spin resonance as a function of frequency. The advantages of such measurements include the following.[7]

1. A Potential Gain in Resolution. Reduction of line width can occur as the frequency is lowered, resulting in the resolution of metal and ligand hyperfine structure, as has been seen in frozen glass spectra of several copper(II) complexes[8,9] and proteins.[10,11] This narrowing can be attributed to a reduction in *g* strain (or correlated *g*–*A* strain[9]), caused by the environment of the electron

(1) (a) La Trobe University. (b) Monash University. (c) Present address: Department of Physics, Monash University. (d) Present address: School of Chemistry, University of N.S.W., Kensington, N.S.W., Australia.
(2) Hyde, J. S.; Froncisz, W. *J. Magn. Reson.* **1982**, *47*, 515.
(3) Hyde, J. S.; Yin, J. J.; Froncisz, W.; Feix, J. B. *J. Magn. Reson.* **1985**, *63*, 142.
(4) Johansson, B.; Haraldson, S.; Pettersson, L.; Beckman, O. *Rev. Sci. Instr.* **1974**, *45*, 1445.
(5) Brown, G. *J. Phys. E* **1974**, *7*, 635.
(6) Dahlberg, E. D.; Dodds, S. A. *Rev. Sci. Instr.* **1981**, *52*, 472.
(7) Froncisz, W.; Hyde, J. S. *Annu. Rev. Biophys. Bioeng.* **1982**, *11*, 391.
(8) Abdrachmanov, R. S.; Ivanova, T. A. *J. Mol. Struct.* **1973**, *19*, 638; **1978**, *46*, 229.
(9) Froncisz, W.; Hyde, J. S. *J. Chem. Phys.* **1980**, *73*, 3123.
(10) Froncisz, W.; Scholes, C. P.; Hyde, J. S.; Wei, Y.-H.; King, T. E.; Shaw, R. W.; Beinert, H. *J. Biol. Chem.* **1979**, *254*, 7482.
(11) Froncisz, W.; Aisen, W. *Biochem. Biophys. Acta* **1982**, *700*, 55.

0002-7863/87/1509-2609$01.50/0

spin varying slightly from molecule to molecule in the strained glassy state.[12]

2. An Increase in Intensity of "Forbidden" Transitions. At low frequencies, nuclear state and/or electronic state mixing can shift the $\Delta M_I = 0$ transitions and increase the transition probabilities of $\Delta M_1 = \pm 1$ and ± 2 transitions.[13]

3. A Redistribution of Spectral Information. To first order, fine, hyperfine (metal and ligand), and quadrupole interactions are independent of frequency whereas g-value resolution is frequency dependent. Consequently, overlap between different spectral features varies with frequency. Such variation has allowed, for example, improved estimation of nuclear quadrupole coupling constants[14] and hyperfine coupling constants and the elimination of "angular anomalies" from the spectra of some Cu(II) species.[9,15,16]

X- and Q-band (ca. 9 and 32 GHz) ESR has proven to be an extremely useful tool for the structural characterization of catalytic intermediates and inhibitor complexes of a number of molybdenum- and tungsten-containing enzymes.[17,18] In order to examine whether increased resolution might obtain at lower frequencies (S band, 2–4 GHz) for Mo(V) and W(V) active sites in these metalloenzymes, a systematic study of structurally well-defined Mo(V) and W(V) complexes was undertaken. The work confirms that the increased resolution observed for copper(II) species extends to these systems. Frequency-dependent ESR spectra are reported for $[Mo^V(abt)_3]^-$ ($abtH_2$ = *o*-aminobenzenethiol) and complexes featuring the $[M^VO]^{3+}$ (M = Mo, W) structural unit bound to various thiolate, selenolate, and Schiff base ligands. These measurements, coupled with ^{95,98}Mo- and ^{17}O-isotope substitution, permit detection of ^{14}N, ^{1}H, ^{17}O, ^{77}Se, and ^{35,37}Cl ligand hyperfine structure in the various compounds. Some aspects of this work have been communicated previously.[19,20]

Experimental Section

Materials. ^{95}Mo and ^{98}Mo were obtained as MoO_3 from Oak Ridge National Laboratory while ^{17}O as H_2O was supplied by the Mound Laboratory. Acetonitrile, methanol, 2-propanol, tetrahydrofuran (THF), and dimethylformamide (DMF)[21] were dried, distilled, and stored anaerobically using standard methods. All solution manipulations were carried out under an atmosphere of purified dinitrogen.

$[Mo(abt)_3]$ ($abtH_2$ = *o*-aminobenzenethiol) and solutions of $[Mo(abt)_3]^-$ were synthesized by the methods of ref 22. $[^{95}Mo(abt)_3]$ was produced by a scaled-down preparation involving $Na_2[^{95}MoO_4]$ (0.1005 g, 0.49 mmol in 6.2 cm^3 of H_2O)[20] and $abtH_2$ (0.22 cm^3, 2 mmol, purified by vacuum distillation). Precipitation of product was maximized by cooling the mixture to 0 °C after reaction and maintaining that temperature during filtration and washing with *i*-PrOH: yield; 0.10 g (44%).

The salts $Et_4N[MO(XPh)_4]$ (M = Mo, W; X = S, Se) were synthesized and isotopically enriched with ^{95}Mo, ^{98}Mo, and ^{17}O according to Hanson.[20] Attempts to prepare ^{95}Mo and ^{98}Mo isotope substituted samples of $[MoO(qtl)_2Cl]$ (qtlH = quinoline-8-thiol) by in situ preparations analogous to those of $[MO(XPh)_4]^-$ were unsuccessful. Consequently, the method of Boyd[23] was scaled down. Synthesis of the Schiff base complexes [MoOL(MeOH)]Br (L = *N*,*N*′-ethane-1,2-diylbis(salicylaldiminato) ("salen") or *N*,*N*′-benzene-1,2-diylbis(salicylaldiminato) ("salophen") and the ^{95}Mo and ^{98}Mo isotopically enriched complex for L = salen (prepared on a semimicroscale) were performed as described by Gheller.[24]

Electron Spin Resonance Measurements. The ESR spectra of all solution samples were measured at room temperature to confirm the presence of a single ESR-active species and subsequently frozen for low-temperature measurements.

At X-band frequencies (ca. 9.1 GHz) measurements were carried out on Varian E-9 and E-12 spectrometers. The low-frequency measurements were carried out using a home-built 1–4-GHz tunable reference arm bridge attached to the E-12 spectrometer. Initially samples were studied in a large rectangular cavity (10 cm × 25 cm × 2.5 cm), with even TE_{012}, TE_{014}, and TE_{015} modes at 1.98, 2.88, and 3.94 GHz, which permitted all three frequencies to be used at any temperature down to ca. 8 K. Later experiments were carired out down to liquid nitrogen temperatures with home-built loop-gap resonators[2] manufactured from Macor ceramic.

Frequencies were measured with an EIP 548-A frequency counter. Magnetic field calibration was obtained via the proton resonance of water. Spectra were recorded on a LSI 11/23 microcomputer coupled to a VAX 11/780 computer.

Computer Simulation of ESR Spectra. Eigenvalues for the spin Hamiltonian (eq 1) with an arbitrary reference frame (triclinic symmetry, nondiagonal **g** and **A** matrices) have been calculated using second-order perturbation theory.[25] The arbitrary reference frame in randomly oriented samples was taken to be the principal g axis system in which **g** is diagonal.

$$\mathcal{H} = \beta \mathbf{B}\cdot\mathbf{g}\cdot\mathbf{S} + \mathbf{S}\cdot\mathbf{A}\cdot\mathbf{I} \quad (1)$$

During the course of this work, the line-width algorithms used in the simulation program have undergone certain changes. Earlier results (reported here), based on the field domain version of the simulation program, have only been retained when the newer program did not result in improved fits or new insights. In order to clarify the position, the two approaches are summarized below.

The conventional approach to simulation of ESR spectra of frozen solution spectra in field-swept experiments[26,27] is to solve the spin-Hamiltonian for the resonance field $B_r(\theta,\phi,M_I)$[25] and to calculate the resulting first-derivative spectrum from the equation

$$S(B) = \int_{\theta=0}^{\theta_m}\int_{\phi=0}^{\phi_m}(\overline{g_1^2}/g)f'(B - B_r,\sigma_B)\,d\cos\theta\,d\phi \quad (2)$$

where $\overline{g_1^2}(\theta,\phi)$ is the powder average value of the transition probability,[27] and σ_B the line width. The presence of g^{-1} is required to effect the transformation from the true transition probability in the frequency domain to the field domain.[28] The first-derivative line-shape function $f'(B)$ is usually taken to be Gaussian but Lorentzian line shapes can also be used. The observed line-width dependence on M_I was treated empirically using the equation:

$$\sigma_{BI} = \alpha_i' + a_i'' + \beta M_{Ii} + \gamma M_{Ii}^2 \quad (3)$$

which is actually most appropriate for Lorentzian line shapes in solution.[29,30]

As a result of a correct understanding of the true nature of field-swept ESR,[31,32] computer simulations can be tackled in the following way. The spin Hamiltonian is solved for energies (or frequencies), and the resonance frequency difference $\nu_0(B)$ as a function of magnetic field is determined at each point across a line. In the absence of g strain (symmetric lines), the line center $\nu_0(B_r) = \nu_c$, is the constant applied frequency. Instead of eq 2, we write

$$S(B) = \int_{\theta=0}^{\theta_m}\int_{\phi=0}^{\phi_m}\overline{g_1^2}f(\nu_c - \nu_0(B),\sigma_\nu)\,d\cos\theta\,d\phi \quad (4)$$

where the line-shape function is defined in frequency space. Here the line width, which itself may vary over a given line, is defined in frequency

(12) Hagen, W. R.; Albracht, S. P. J. *Biochem. Biophys. Acta* **1982**, *702*, 61.
(13) Smith, T. D.; Pilbrow, J. R. *Coord. Chem. Rev.* **1974**, *13*, 173.
(14) Liczwek, D. L.; Belford, R. L.; Pilbrow, J. R.; Hyde, J. S. *J. Phys. Chem.* **1983**, *87*, 2509.
(15) Ovchinnikov, I. V.; Konstantinov, J. *J. Magn. Reson.* **1978**, *30*, 179.
(16) Bonomo, R. P.; Riggi, F. *Lett. Nuovo Cimento* **1981**, *30*, 304.
(17) Bray, R. C. *Biol. Magn. Reson.* **1980**, *2*, 45.
(18) *Molybdenum and Molybdenum Containing Enzymes*; Coughlan, M. P., Ed.; Pergamon Press: Oxford, 1980.
(19) Farchione, F.; Hanson, G. R.; Rodrigues, C. G.; Bailey, T. D.; Bagchi, R. N.; Bond, A. M.; Pilbrow, J. R.; Wedd, A. G., *J. Am. Chem. Soc.* **1986**, *108*, 831.
(20) Hanson, G. R.; Brunette, A. A.; McDonell, A. C.; Murray, K. S.; Wedd, A. G. *J. Am. Chem. Soc.* **1981**, *103*, 1953.
(21) (a) Juillard, J. *Pure Appl. Chem.* **1977**, *49*, 885. (b) Burfield, D. R.; Smithers, R. H. *J. Org. Chem.* **1978**, *43*, 3966.
(22) Gardner, J. K.; Pariyadath, N.; Corbin, J. L.; Stiefel, E. I., *Inorg. Chem.* **1978**, *17*, 897.
(23) Boyd, I. W.; Wedd, A. G. *Aust. J. Chem.* **1984**, *37*, 293.
(24) Gheller, S. F.; Bradbury, J. R.; Mackay, M. F.; Wedd, A. G. *Inorg. Chem.* **1981**, *20*, 3899.
(25) (a) Lin, W. C. *Mol. Phys.* **1973**, *25*, 247. (b) Freeman, T. E. Ph.D. Thesis, Monash University, 1973.
(26) Toy, A. D.; Chaston, S. H. H.; Pilbrow, J. R.; Smith, T. D. *Inorg. Chem.* **1971**, *10*, 2219.
(27) Pilbrow, J. R.; Winfield, M. E. *Mol. Phys.* **1973**, *25*, 1073.
(28) Aasa, R.; Vanngard, T. *J. Magn. Reson.* **1975**, *19*, 308.
(29) (a) Kivelson, D. *Electron Spin Relaxation in Liquids*; Muus, L. T., Atkins, P. W., Eds.; Plenum Press: New York, 1972; p 213. (b) Atkins, P. W. *Ibid.* p 279.
(30) Wilson, R.; Kivelson, D. *J. Chem. Phys.* **1966**, *44*, 154, 4445.
(31) Pilbrow, J. R. *J. Magn. Reson.* **1984**, *58*, 186.
(32) Pilbrow, J. R.; Sinclair, G. R.; Hutton, D. R.; Troup, G. J. *J. Magn. Reson.* **1983**, *52*, 386.

Table I. ESR Parameters[a]

Axial Systems

species	$\langle g \rangle$	$\langle A \rangle$	$g_\parallel$	$g_\perp$	$A_\parallel$	$A_\perp$	ligand L	$\langle A^L \rangle$	$A_\parallel^L$	$A_\perp^L$
$[Mo(abt)_3]^{-b}$	1.990	33.8	1.990	1.990	11.9	45.1	^{14}N	1.9	*c*	*c*
							^{1}H	5.8	*c*	*c*
$[MoOCl_4]^{-d}$	1.956	52.5	1.9670	1.950	79.0	39.0				
$[MoO(SPh)_4]^{-e}$	1.990	32.3	2.017	1.979	52.3	22.3	^{17}O	2.12	0.64	2.86
$[MoO(SePh)_4]^{-e}$	2.024	30.0	2.072	2.005	48.3	21.2	^{77}Se	−4.56	+16.9	−15.0
							^{17}O	2.1		
$[WO(SPh)_4]^{-e}$	1.936	55.1	2.018	1.903	78.1	44.4				
$[WO(SePh)_4]^{-e}$	1.971	50.6	2.086	1.923	74.0	43.3	^{77}Se		18.3	

Nonaxial Systems

	$\langle g \rangle$	$\langle A \rangle$	g_3	g_1, g_2	A_z	A_x, A_y	ligand L	$\langle A^L \rangle$	A_z^L	A_x^L, A_y^L
$[MoO(salen)(DMF)]^{+f}$	1.943	40.2	1.960	1.925	24.0	31.5				
				1.945		70.4				
$[MoO(qtl)_2Cl]^g$	1.970	40.9	2.006	1.953	60.7	24.1	$^{35,37}Cl$	2	<0.3	6.7
				1.952		31.9				<0.3

[a] The **g**, hyperfine, and superhyperfine matrices were refined using computer simulation. The molybdenum hyperfine matrix was determined from ^{95}Mo-enriched samples. Except for $[Mo(abt)_3]^-$, the **g** and superhyperfine matrices were determined from ^{98}Mo-enriched samples. Units of hyperfine parameters: 10^{-4} cm^{-1}. [b] Solvent is THF. Line-width parameters (eq 5): $\sigma_{Rx,y}$, 27.02 MHz; $C_{1x,y}$, 0.0008; $C_{2x,y}$, 11.359; σ_{Rz}, 22.28 MHz; $C_{1z} = C_{2z} = 0.0$. [c] Assumed to be isotropic in the computer simulation. [d] Solvent is DMF: Garner, C. D.; Hyde, M. R.; Mabbs, F. E. *Inorg. Chem.* **1976**, *15*, 2327. [e] Solvent is 4:1 (v:v) MeCN/DMF. [f] Solvent is DMF (0.1 M Et_4NPF_6). An angle of 30 (±5)° between g_1 and A_x and g_2 and A_y. Line-width parameters (eq 5): σ_{Rx}, 17.24 MHz; σ_{Ry}, 12.25 MHz; σ_{Rz}, 10.97 MHz; $C_{1i} = C_{2i} = 0.0$ ($i = x, y, z$). [g] Solvent is CH_2Cl_2. The ligand hyperfine and **g** matrices were assumed to coincide in the simulation of the ^{98}Mo-enriched spectra. The ^{95}Mo hyperfine matrix given in the table was obtained from the best simulation of the ^{95}Mo-enriched spectrum at 4 GHz. In this simulation **g** and **A** were assumed to be coincident.

units. Note the absence of the g^{-1} factor which has no place in eq 4. Algorithms based on eq 4 are a little slower than those using eq 2. In place of eq 3, fitting of σ is based on the ideas of Froncisz and Hyde[9] but reinterpreted in frequency domain language.[31] Based upon a perfect correlation between g_i and A_i ($i = x, y, z$), we can write for orthorhombic symmetry:

$$\sigma_i = [\sigma_{Ri}^2 + (C_{1i}\nu_0(B) + C_{2i}M_I)^2]^{1/2} \quad (5)$$

where σ_R is the residual line width due to spin–spin broadening and unresolved ligand hyperfine structure. If σ_g and σ_A are variances in the x, y, and z components of g and A, respectively, then we may write

$$C_1 = \sigma_g/g \text{ and } C_2 = \sigma_A$$

The angular variation, for purposes of frozen-solution spectral simulations, is treated at if it were a hyperfine structure:

$$\sigma_\nu^2 = \Sigma\sigma_i^2 l_i^2 \qquad i = x, y, z \quad (6)$$

where l_i are the direction cosines. This is a limitation but is a common assumption in ESR fitting. It gives correct values along principal axes but not necessarily along other orientations.

While excellent fits for certain Cu(II) or low-spin Co(II) spectra have been obtained at X band[33] and sometimes at S band,[34] it has not proven possible to obtain comparable fits to spectra at two or more frequencies with a single set of parameters. Fitting of certain spectra in this paper (especially those of $[MoO(qtl)_2X]$ (X = Cl, Br)) indicate that a more refined model is required, possibly along the lines of the g-strain model successfully used for iron–sulfur proteins by Hagen et al.[35]

Results and Discussion

Typical ESR spectra of Mo(V) and W(V) species in liquid solution include a central absorption due to resonance of molecules with metal isotopes of zero nuclear spin ($I = 0$). This is flanked by hyperfine lines due to resonance of molecules with metal isotopes of nonzero nuclear spin ($I \neq 0$). There are six hyperfine lines for molybdenum due to the presence of ^{95}Mo (15.72 atom %, $I = {}^5/_2$, $\mu = -0.9133\ \beta_N$) and ^{97}Mo (9.46 atom %, $I = {}^5/_2$, $\mu = -0.9325\ \beta_N$). See, for example, Figure 2a. The individual contributions are unresolved normally. There are two hyperfine lines for tungsten due to the presence of ^{183}W (14.40 atom %, $I = {}^1/_2$, $\mu = +0.1172\ \beta_N$). A summary of the ESR parameters derived in the present work is given in Table I.

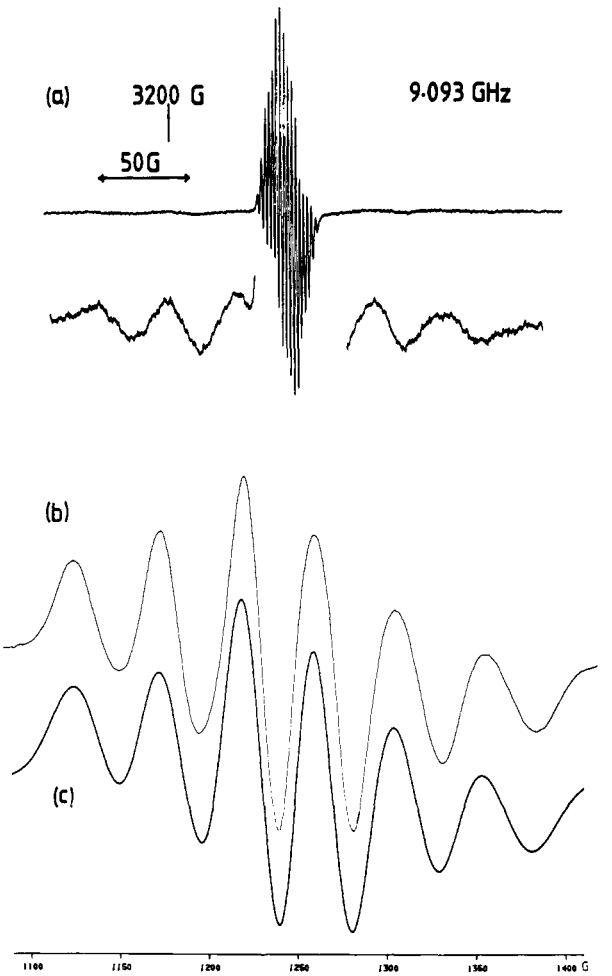

Figure 1. ESR spectrum of $[Mo(abt)_3]^-$ in THF: (a) 189 K, 9.093 GHz; (b) 77 K, 3.479 GHz, ^{95}Mo 96.47 atom %; (c) simulation of (b).

$[Mo(abt)_3]^-$ in THF. Solutions generated at a concentration of 12 mM exhibit no ^{14}N or ^{1}H superhyperfine structure on the $I = 0$ transition at room temperature, presumably because of exchange broadening. However, samples appear to degrade slowly at room temperature and, after about 12 h, partially resolved structure appears. Measurements reported here are on solutions

(33) (a) Dougherty, G.; Pilbrow, J. R.; Skorobogaty, A.; Smith, T. D. *J. Chem. Soc., Dalton Trans.* **1985**, *81*, 1739. (b) Skorobogaty, A.; Smith, T. D.; Pilbrow, J. R.; Rawlings, S. J. *J. Chem. Soc., Faraday Trans. 2* **1986**, *82*, 173.

(34) Rakhit, G.; Antholine, W.; Froncisz, W.; Hyde, J. S.; Pilbrow, J. R.; Sinclair, G. R.; Sarker, B. *J. Inorg. Biochem.* **1985**, *5*, 217.

(35) (a) Hagen, W. R.; Hearshen, D. O.; Sands, R. H.; Dunham, W. R., *J. Magn. Reson.* **1985**, *61*, 220. (b) Hagen, W. R.; Hearshen, D. O.; Harding, L. J.; Dunham, W. R. *Ibid.* **1985**, *61*, 233.

which exhibit the best resolution. The spectra are indistinguishable from those generated at lower concentrations, but are more intense.

Resolution of the $I = 0$ resonance is enhanced[22] in liquid solution at lower temperatures (−40 to −90 °C). A 16-line spectrum with peak-to-peak line widths of about 1 G is observed (Figure 1a), and spectral simulation is consistent with the presence of three equivalent ^{14}N and three equivalent ^{1}H nuclei.[22] In the present work, values of $\langle A(^{14}N)\rangle$ (1.9×10^{-4} cm^{-1}) and $\langle A(^{1}H)\rangle$ (5.8×10^{-4} cm^{-1}) furnished the best simulation using eq 4. The results are consistent with the presence of an $[Mo(abt)_3]^-$ anion with C_3 point symmetry, of which the extreme stereochemistries are trigonal prismatic and *facial* octahedral (chelate twist angles are 0 and 60°, respectively). The oxidized species $[Mo(abt)_3]$ has a twist angle of 12° in the solid state.[36] The enhanced resolution at low temperature suggests that a single conformer is present below −40 °C.

At room temperature, the hyperfine lines are broader than the $I = 0$ line. As the temperature decreases, the hyperfine lines narrow and ^{14}N and ^{1}H structure is resolved partially at −30 °C. However, in contrast to the behavior of the $I = 0$ resonance, the hyperfine line widths increase below −30 °C and are difficult to detect at −84 °C (Figure 1a). The observations are consistent with the major spin relaxation mechanism being associated with the fluctuating fields present in the tumbling molecule in solution due to anisotropy in the **g** and **A** matrices.[20,29,30] The highly isotropic **g** matrix (vide infra, Table I) in $[Mo(abt)_3]^-$ means that the $I = 0$ line is not broadened significantly as the rate of tumbling decreases at lower temperatures, while the highly anisotropic **A** matrix leads to significant broadening of the hyperfine lines.

In frozen solution, a single derivative feature is seen for the $I = 0$ transition and a peak-to-peak line width of 83.6 MHz at a microwave frequency of 34.6 GHz predicts a maximum g anisotropy of 0.005 only. Isotope enrichment with ^{95}Mo (96.47 atom %) allows examination of the $I = {}^5/_2$ transitions (Figure 1b). The spectra are essentially independent of frequency (9.1, 3.5, and 2.5 GHz) which confirms the isotropic nature of the **g** tensor.

Satisfactory spectral simulation (Figure 1c) at all frequencies is possible assuming an isotropic **g** matrix, an axial $\mathbf{A}(^{95,97}Mo)$ matrix, and isotropic $\mathbf{A}(^{14}N)$- and $\mathbf{A}(^{1}H)$ matrices (Table I):

$$\mathcal{H} = \beta g \mathbf{B}\cdot\mathbf{S} + A_\parallel S_z I_z + A_\perp(S_x I_x + S_y I_y) + A^N \mathbf{S}\cdot\mathbf{I}^N + A^H \mathbf{S}\cdot\mathbf{I}^H \quad (7)$$

where the parameters have their usual ESR meaning. In particular, $A_\parallel < A_\perp$, which contrast with the behavior of hyperfine coupling for the $[MO(XPh)_4]^-$ anions discussed below.

A qualitative theoretical analysis[37] has helped to rationalize the experimental observation that low numbers of d electrons (d^0–d^2) favor trigonal prismatic coordination. With z as the threefold axis, a d_{z^2}-based ground state is likely and then, to a first approximation,[38]

$$A_\parallel \cong P[-K + {}^4/_7] \quad (8a)$$

$$A_\perp \cong P[-K - {}^2/_7] \quad (8b)$$

where $P = 2g_N\beta_e\beta_N\langle r^{-3}\rangle_d$ and K is the core polarization parameter. Since $K \sim 0.9$ is reasonable for molybdenum,[39] $|A_\parallel|$ will always be smaller than $|A_\perp|$, as observed for $[Mo(abt)_3]^-$ (Table I).

$[MO(XPh)_4]^-$ (M = Mo, W; X = S, Se). *g* Values and Hyperfine Coupling Constants. Liquid and frozen solution spectra of the four anions $[MO(XPh)_4]^-$ (M = Mo, W; X = S, Se) have been examined[20] previously at X-band (ca. 9 GHz) frequencies. Enrichment of naturally abundant molybdenum with ^{98}Mo ($I = 0$) removes $^{95,97}Mo$ hyperfine lines from the spectra. The presence of a single species is readily confirmed in solution and the frozen solution spectrum is simplified for easy extraction of the g values (for example, Figure 3a).

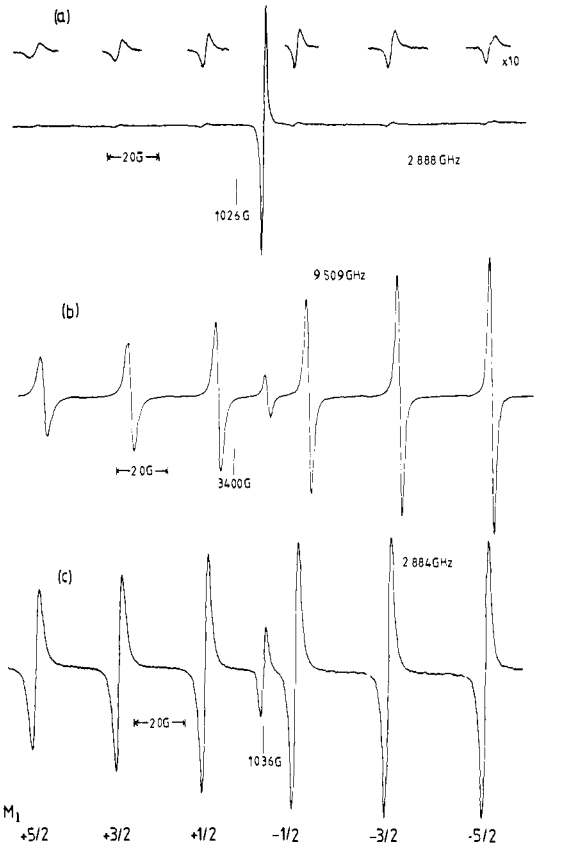

Figure 2. ESR spectra of $[MoO(SPh)_4]^-$ in 4:1 MeCN/DMF at 300 K: (a) 2.888 GHz; (b) ^{95}Mo 96.47 atom%, 9.509 GHz; (c) ^{95}Mo 96.47 atom%, 2.884 GHz.

Solution spectra at 9.509 and 2.884 GHz of ^{95}Mo-enriched $[MoO(SPh)_4]^-$ are shown in Figure 2b,c. To first order, the hyperfine splittings are independent of the magnetic field. However, as the frequency is lowered, the resonant field positions of the hyperfine lines can be seen to shift downfield relative to that of the central ($I = 0$) line owing to the influence of second-order perturbation terms which depend inversely on the magnetic field.[25] This leads to slight differences in the estimates of g values derived from central ($I = 0$) transitions (where such second-order terms do not apply) and the hyperfine ($I = {}^5/_2$) lines. Such variations (±0.002) are significant when simulating spectra.

The anisotropic spectra of these square-pyramidal d^1 anions[20,40] may be described by an axial spin Hamiltonian:

$$\mathcal{H} = \beta[g_\parallel B_z S_z + g_\perp(B_x S_x + B_y S_y)] + A_\parallel S_z I_z + A_\perp(S_x I_x + S_y I_y) \quad (9)$$

Satisfactory simulation of the ESR spectra from each anion at each frequency was achieved (Table I) employing eq 2 (see, for example, Figure 3 and ref 41). Although simulations were required to determine $A_\perp$ at X band,[20] that parameter can be readily estimated from the S band spectra (Figure 3b).

The present status of the theory relating the spin-Hamiltonian parameters to LCAO molecular orbital theory for d^1 ions with C_{4v} symmetry has been presented by DeArmond.[39] In summary, the ground state $|B_2\rangle$ and antibonding molecular orbitals with B_1 and E symmetry respectively can be described by:

$$|B_2\rangle = a|xy\rangle - a'|\phi\rangle \quad (10a)$$

$$|E\rangle = b|yz,xz\rangle - b'|\phi\rangle \quad (10b)$$

$$|B_1\rangle = c|x^2 - y^2\rangle - c'|\phi\rangle \quad (10c)$$

where ϕ represents a linear combination of ligand atomic orbitals

(36) Yamanouchi, K.; Enemark, J. H. *Inorg. Chem.* **1978**, *17*, 2911.
(37) Hoffmann, R.; Howell, J. M.; Rossi, A. R. *J. Am. Chem. Soc.* **1976**, *98*, 2484.
(38) Goodman, B. A.; Raynor, J. B. *Adv. Inorg. Radiochem.* **1970**, *13*, 135.
(39) DeArmond, K.; Garett, B. B.; Gutowsky, H. S., *J. Chem. Phys.* **1965**, *42*, 1019.
(40) Bradbury, J. R.; Mackay, M. F.; Wedd, A. G. *Aust. J. Chem.* **1978**, *31*, 2423.
(41) Hanson, G. R. Ph.D. Thesis, La Trobe University, 1984.

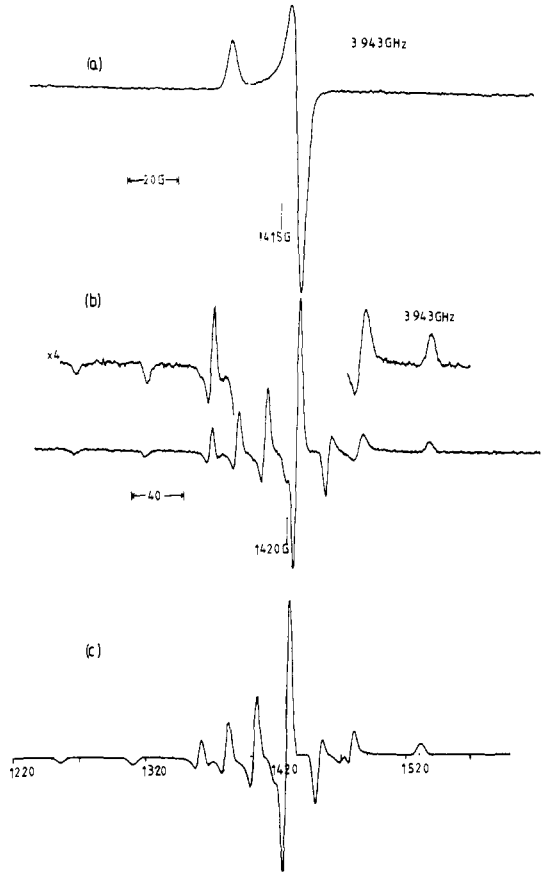

Figure 3. ESR spectra of $[MoO(SPh)_4]^-$ in 4:1 MeCN/DMF at 77 K and 3.943 GHz: (a) ^{98}Mo 98.32 atom %; (b) ^{95}Mo 96.47 atom %; (c) simulation of (b).

of appropriate symmetry. The g and A values can then be calculated:

$$g_\parallel = g_e - [4(2\lambda_M ac - \lambda_L a'c')/(E_{B1} - E_{B2})] \quad (11a)$$

$$g_\perp = g_e - [2\lambda_M ab/(E_E - E_{B2})] \quad (11b)$$

$$A_\parallel = -P[a^2(K + 4/7)] \quad (12a)$$

$$A_\perp = -P[a^2(K - 2/7)] \quad (12b)$$

where λ_M and λ_L are the spin–orbit coupling constants of the metal and ligands, and E_j (j = B_2, B_1, E) is the energy of the jth molecular orbital in eq 10. Clearly the observed increase in $g_\parallel$ and $g_\perp$ and the decrease in $A_\parallel$ and $A_\perp$ (Table I) as the ligating atoms change from chlorine to sulfur to selenium in both the molybdenum and tungsten complexes can be attributed to an increase in the ligand spin–orbit coupling constants (λ_L, L = Cl, 152 cm^{-1}; L = S, 382 cm^{-1}; and L = Se, 1690 cm^{-1})[42,43] and the decrease in the molecular orbital coefficients (a, b, c). The relative magnitudes of the g and A values, $g_\parallel > g_\perp$ and $|A_\parallel| > |A_\perp|$, are reflected in eq 11 and 12, respectively, and contrast with those for $[Mo(abt)_3]^-$.

Line Widths. Examination[20] of the peak-to-peak line widths, σ_B, of the hyperfine lines of $[MoO(SPh)_4]^-$ in liquid solution as a function of temperature and frequency (X and Q band) showed that the major spin relaxation mechanism is associated with anisotropy in the **g** and **A** matrices[29,30] and that the line width is determined by eq 3 with a Lorentzian line shape. Now, the parameters α' and β of eq 3 are proportional to B^2 and B, respectively,[29,30] so the line widths of the central (I = 0) and hyperfine lines in liquid solution should decrease as the frequency is lowered. This is confirmed experimentally for $[MoO(XPh)_4]^-$ ions in the present work. For example, the line width of the I =

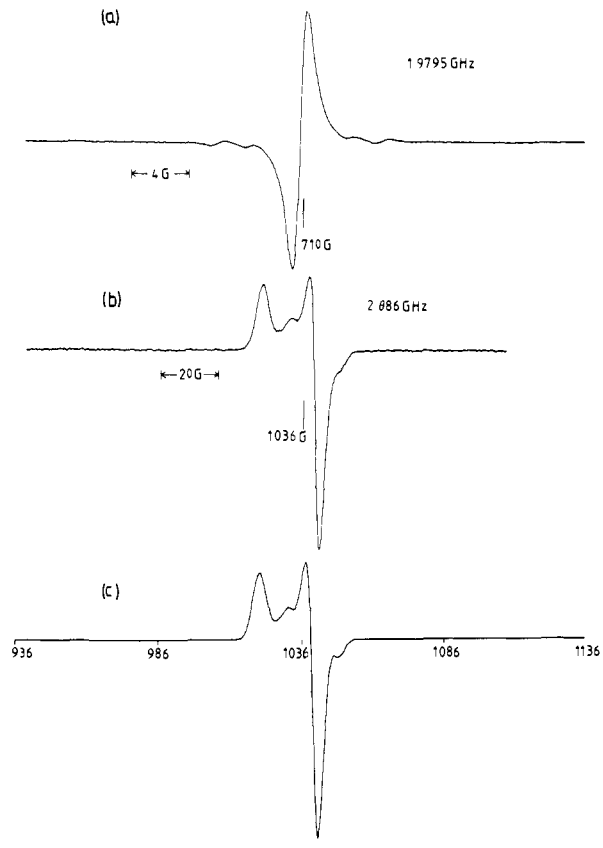

Figure 4. ESR spectra of $[MoO(SPh)_4]^-$ (^{98}Mo 98.23 atom %; ^{17}O 24.90 atom %): (a) MeCN, 300 K, 1.9795 GHz; (b) 4:1 MeCN/DMF, 77 K, 2.886 GHz; (c) simulation of (b).

0 transition in $[WO(SPh)_4]^-$ is reduced from 32.5 MHz at 9.4 GHz to 23.9 MHz at 2.9 GHz and from 11.6 to 6.8 MHz in $[MoO(SePh)_4]^-$. On the other hand, the individual ^{95}Mo and ^{97}Mo hyperfine lines are partially resolved on the $M_I = -5/2$ component in naturally abundant $[MoO(SPh)_4]^-$ at 2.9 GHz (Figure 2a), but not at higher frequencies.

The frozen solution spectra of $[MO(XPh)_4]^-$ are also narrowed significantly when the frequency is lowered (compare Figure 3 with that of Figure 3, ref 20). This narrowing can be attributed to a reduction in g and A strain.[9]

Ligand Hyperfine Coupling Constants. The reduction in line widths at lower frequencies in both the liquid and the frozen solution spectra has allowed resolution of ligand hyperfine interactions present in certain compounds. For example, weak ^{17}O coupling has been observed[20,44,45] in the X-band liquid solution spectrum of $[MoO(SPh)_4]^-$. The better resolution at 1.9795 GHz permits observation[46] of four of the six hyperfine lines (Figure 4a). This structure is not resolved in the X-band frozen solution spectrum although broadening of the perpendicular feature is apparent.[20,44] However, at low frequency, the structure is resolved (Figure 4b), and simulation of spectra derived at four frequencies (1.98, 2.88, 3.8, 9.1 GHz, Figure 4c) allows extraction of the anisotropic ^{17}O hyperfine parameters ($A_\parallel$, 0.64 × 10^{-4} cm^{-1}; $A_\perp$, 2.86 × 10^{-4} cm^{-4}).

These parameters span the range (0.6–2.9 × 10^{-4} cm^{-1}) observed[47] for the formaldehyde-inhibited signal of xanthine oxidase. The low magnitude of the coupling and its anisotropy lends weight to the suggestion that this form of the enzyme features a terminal oxo ligand oriented with its valence orbitals essentially orthogonal to the molybdenum-based magnetic orbital. A similar situation

(42) Keijzers, C. P.; DeBoer, E. *Mol. Phys.* **1979**, *38*, 209.
(43) McClure, D. S. *J. Chem. Phys.* **1949**, *47*, 905.
(44) Cramer, S. P.; Johnson, S. L.; Rajagopalan, K. V.; Sorrell, T. N., *Biochem. Biophys. Res. Commun.* **1979**, *91*, 434.
(45) Miller, K. F.; Stiefel, E. I., personal communication to: Gutteridge, S.; Malthouse, J. P. G.; Bray, R. C. *J. Inorg. Biochem.* **1979**, *11*, 355.
(46) The ^{17}O superhyperfine structure disappeared after about 0.3 h at room temperature owing to exchange with residual $H_2{}^{16}O$ in the solvent.
(47) Bray, R. C.; Gutteridge, S. *Biochemistry* **1982**, *21*, 5992.

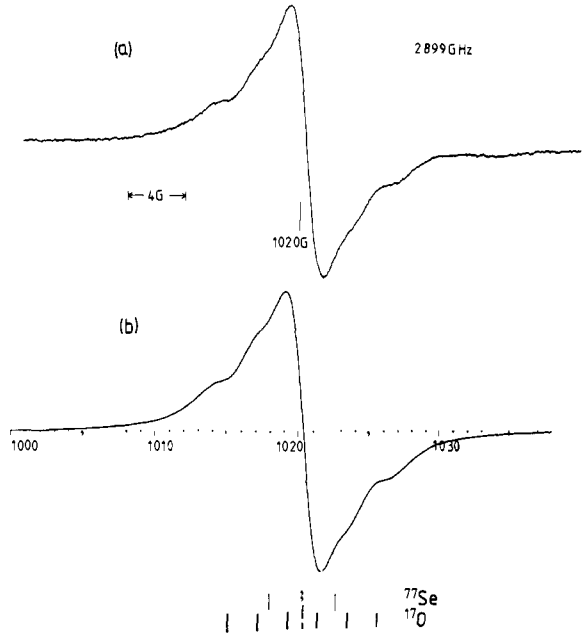

Figure 5. ESR spectrum of $[MoO(SePh)_4]^-$ in MeCN at 300 K and 2.899 GHz: (a) ^{98}Mo 98.23 atom %, ^{17}O 24.90 atom %; (b) simulation of (a).

seems to apply to the arsenite-inhibited enzyme[48]. These cases contrast with other forms of the enzyme (including its active form) where larger coupling constants ($8-16 \times 10^{-4}$ cm^{-1}) are observed.[47,48] Synthesis[19] of *cis*-$[MoO(OH)L^1]$ (L^1H_2 = $(HSCH_2CH_2NMeCH_2)_2$) indicates that a hydroxy ligand is the source of the larger coupling constants in some forms.

^{77}Se and ^{17}O hyperfine coupling can be detected in the ESR spectra of $[MoO(SePh)_4]^-$. The line widths of the hyperfine lines in liquid solution do not obey[49] eq 3, apparently because of the presence of unresolved ^{77}Se hyperfine coupling (^{77}Se, $I = {}^1/_2$; 7.58 atom %). Similar effects have been observed[29,50] in diselenophosphate and related Cu(II) complexes. The ^{77}Se coupling ($|\langle A \rangle| = 4.56 \times 10^{-4}$ cm^{-1}) was detected directly in ^{98}Mo-enriched $[MoO(SePh)_4]^-$ at 2.899 GHz, as was ^{17}O coupling ($|\langle A(^{17}O) \rangle| = 2.1 \times 10^{-4}$ cm^{-1}) in ^{17}O-enriched samples (Figure 5). While the ^{17}O structure could not be detected in frozen solution spectra owing to the larger linewidths, the ^{77}Se structure was readily detected at 2.9 and 2.0 GHz owing to the magnitude of the anisotropic components ($|A_\parallel| = 16.9$, $|A_\perp| = 15.0 \times 10^{-4}$ cm^{-1}).

Standard arguments[38] suggest that $\langle A(^{77}Se) \rangle$ is negative implying that $A_\parallel$ is positive and $A_\perp$ negative and that the anisotropic component $A_P = +10.8 \times 10^{-4}$ cm^{-1}. As the direct dipole–dipole contribution to A_p is calculated to be -126×10^{-4} cm^{-1} using a point dipole model,[38] a large and positive covalent contribution is required to explain the observed value of A_P. This can be attributed to direct $d_\pi - p_\pi$ overlap between Mo ($4d_{xy}$) and Se (4p) valence orbitals (cf., eq 10a).

Lowering the frequency from X to S band increases the resolution of ^{183}W hyperfine coupling in $[WO(XPh)_4]^-$ (X = S, Se; Figure 6). Resolution of ^{77}Se structure is also observed, but only on the parallel component. This is a result of the larger line widths in these species caused by increased g and A strain as a result of the greater anisotropy in the **g** and **A** matrices (Table I) relative to the molybdenum analogues.

$[MoOL(DMF)]^+$ (L = salen, salophen). Equilibria between mononuclear and polynuclear species exist[24,52] in solutions of

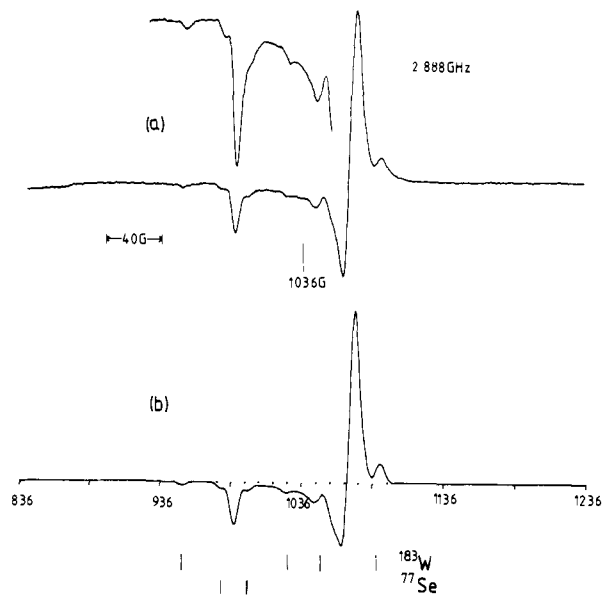

Figure 6. ESR spectrum of $[WO(SePh)_4]^-$: (a) 4:1 MeCN/DMF, 77 K, 2.888 GHz; (b) simulation of (a).

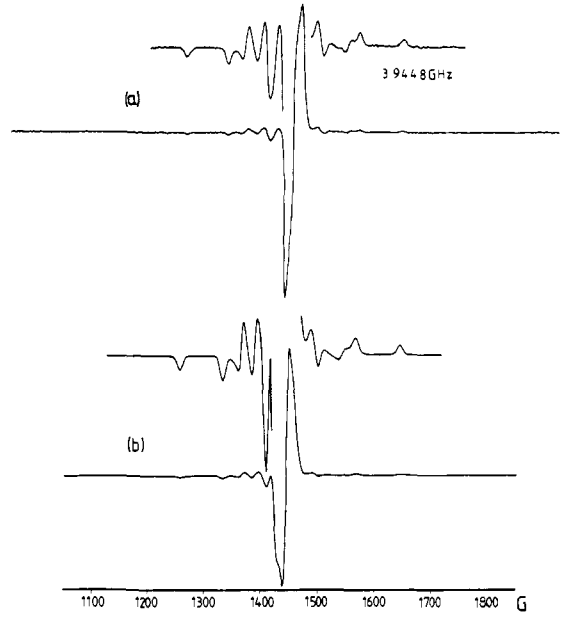

Figure 7. ESR spectrum of *trans*-$[MoOL(DMF)]^+$ (L = salen) obtained by dissolving [MoOL(MeOH)]Br in DMF (0.1 M Et_4NPF_6): (a) 77 K, 3.9448 GHz; (b) simulation of (a).

trans-[MoOL(MeOH)]Br where L are certain quadridentate Schiff base ligands. However, 4 mM solutions of recrystallized materials in DMF (0.1 M Et_4NPF_6) contain a single ESR-active species in the salophen case and the relative concentration of a second species is less than 4% in the salen case. The frozen solution spectra are very similar in both examples and are assigned to the *trans*-$[MoOL(DMF)]^+$ (C_s local point symmetry) in view of the rigid planar structure of the salophen ligand. The frozen solution spectra can be described by the monoclinic spin Hamiltonian

$$\mathcal{H} = \beta \Sigma g_i B_i S_i + \Sigma A_j S_j I_j \; (i = 1, 2, 3; j = x, y, z) \quad (13)$$

In C_s symmetry, the unique magnetic axis (g_3,A_z) is normal to the mirror plane σ_{xz} and corresponds to the molecular y axis which lies between the metal–ligand bonds.

Isotope substitution and computer simulation using eq 3 were employed to determine the monoclinic **g** and **A** matrixes at Q-, X-, and S-band frequencies (Figure 7; Table I). Satisfactory simulation of the ^{95}Mo spectra was obtained only when an angle of 30 (±5)° was included between g_1 and A_x and between g_2 and

(48) George, G. N.; Bray, R. C. *Biochemistry* **1983**, *22*, 1013.
(49) The parameter γ does not vary as η/T (c = dielectric constant) in MeCN as required by theory.[29]
(50) Prabhanandra, B. S. *Mol. Phys.* **1979**, *38*, 209.
(51) Kuska, H. A.; Rogers, M. T. In *Radical Ions*; Kaiser, E. T., Ed.; Wiley-Interscience: New York, 1968; p 579.
(52) Bradbury, J. R.; Hanson, G. R.; Bond, A. M.; Wedd, A. G. *Inorg. Chem.* **1984**, *23*, 844.

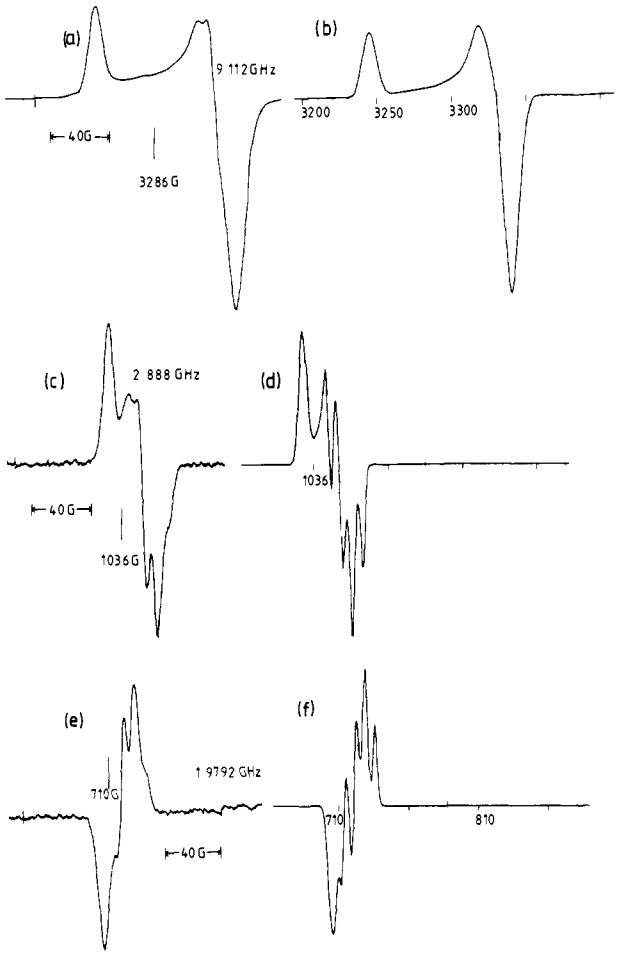

Figure 8. ESR spectra of $[MoO(qtl)_2Cl]$ (^{98}Mo 98.23 atom %) in DMF at 77 K: (a) 9.112 GHz, (b) simulation of (a), (c) 2.888 GHz, (d) simulation of (c), (e) 1.9792 GHz, (f) simulation of (e).

A_y. The inclusion of this angle reflects the monoclinic symmetry (C_s) of the molybdenum site in this complex. Interestingly the simulated ESR spectra of [MoO(salophen)Cl][53] did not require the inclusion of such an angle.

Spin–orbit coupling of the predominantly ground-state molecular orbital $|x^2 - y^2\rangle$ (which transforms as A') to the excited state $|xz\rangle$(A′) can result in rotation of the g_1 and A_x and g_2 and A_y components about the molecular y axis.[53-56]

***cis*-[MoO(qtl)$_2$X] (X = Cl, Br).** The spectrum of the chloro species has an interesting history. It was reported[57] initially to be similar to that of the "very rapid" signal of xanthine oxidase. Isolation of the crystalline compound and its doping[53] into the diamagnetic isostructural host *cis*-$[MoO_2(qtl)_2]$ demonstrated that its bona fide spectrum was quite different from that of the initial report. The **g** and **A**($^{95-97}$Mo) matrices were estimated[53] by spectral simulation assuming monoclinic (C_s) symmetry with an angle of 10° between the g_1 and A_x components of the **g** and **A** matrices.

In the present work, observation of $[MoO(qtl)_2Cl]$ enriched to 98.73 atom % in ^{98}Mo at five frequencies (34.8, 9.1, 3.9, 2.9, and 2.0 GHz) (Figure 8) demonstrates that the structure on the high-field $I = 0$ resonance is independent of frequency and is a result of coupling to a single chloride ($I = {}^3/_2$) ligand.[58] In consequence, the previous simulation[53] must be revised. Computer simulations employing eq 3 are adequate (Figure 8), allowing extraction of rhombic **g** and **A**(^{35,37}Cl) matrices (Table I).

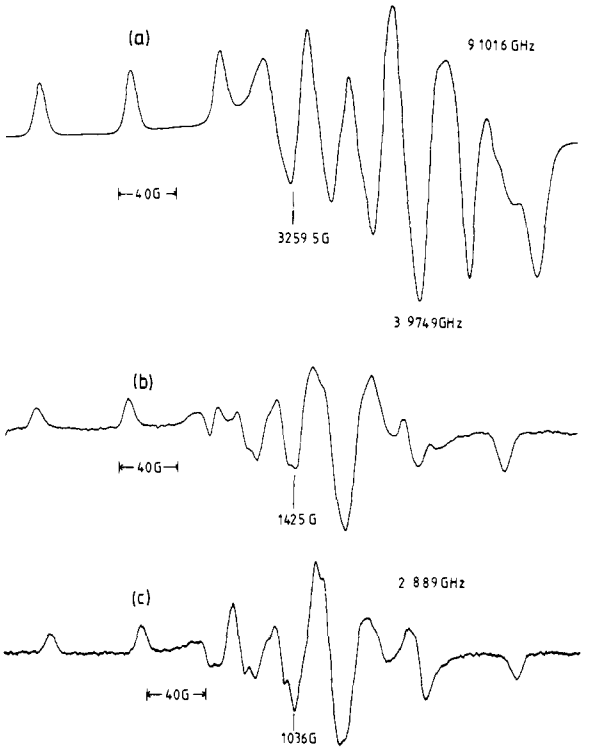

Figure 9. ESR spectra of $[MoO(qtl)_2Cl]$ (^{95}Mo 96.4m atom %) in DMF at 77 K: (a) 9.1016 GHz, (b) 3.9749 GHz, (c) 2.889 GHz.

While the liquid solution spectrum of $[^{95}MoO(qtl)_2Cl]$ (96.47 atom % ^{95}Mo) provides $\langle A(^{95}Mo)\rangle$ and the frozen solution spectra of 34.8, 9.1, 3.9, and 2.9 GHz are of good quality (Figure 9), simulation to extract the hyperfine matrix components and their orientation relative to the **g** matrix has not been achieved to a satisfactory standard (see Experimental Section). No single parameter set simulated the observed spectra at all frequencies. The potential problems of parameter estimation by simulation at a single frequency are illustrated well by this example. The hyperfine parameters quoted in Table I are those which gave the most satisfactory simulation at 3.97 GHz.

The corresponding bromide salt has been isolated[23] and its ESR spectrum recorded. Notably, the X-band solution spectrum shows resolved ^{79,81}Br superhyperfine structure ($\langle A\rangle$, 7×10^{-4} cm^{-1}). The larger superhyperfine coupling constant for bromine relative to chlorine (2×10^{-4} cm^{-1}) can be attributed to the greater nuclear magnetic moment and an increase in convalency. Unfortunately anisotropic spectra could not be obtained, as solvents such as DMF and MeCN, which give good glasses at 77 K, show at least two species at room temperature. The presence of the two species may be explained by an equilibrium involving $[MoO(qtl)_2Br]$ and $[MoO(qtl)_2(DMF)]^+$ Br^- in which the second species does not exhibit bromine superhyperfine coupling (results not shown).

Conclusions

Improved resolution results from the reduction in line width observed for spectra of molybdenum(V) and tungsten(V) species recorded at the lower microwave frequencies (2–4 GHz) and is observed in both isotropic and anisotropic spectra. For the latter, a reduction in g and A strain is the major reason, while in the former line-width parameters are direct functions of the magnetic field. In particular, ^{17}O, ^{77}Se, and ^{35,37}Cl superhyperfine interactions are detected for $[MO(XPh)_4]^-$ (M = Mo, W; X = S, Se) and *cis*-$[MoO(qtl)_2Cl]$. The anisotropic ^{17}O superhyperfine parameters of $[MoO(SPh)_4]^-$ span those observed for the formal-

(53) Scullane, M. I.; Taylor, R. D.; Minelli, M.; Spence, J. T.; Yamanouchi, K.; Enemark, J. H.; Chasteen, N. D. *Inorg. Chem.* **1979**, *18*, 3213.
(54) Pilbrow, J. R.; Lowrey, M. R. *Rep. Prog. Phys.* **1980**, *43*, 433.
(55) Hitchman, M. A.; Olson, C. D.; Belford, R. L. *J. Chem. Phys.* **1969**, *50*, 1195.
(56) Belford, R. L.; Harrowfield, B.; Pilbrow, J. R. *J. Magn. Reson.* **1977**, *28*, 433.
(57) (a) Marov, I. N.; Belyaeva, V. K.; Dubrov, Y. N.; Ermarkov, A. N. *Russ. J. Inorg. Chem. (Engl. Trans.)* **1972**, *17*, 515. (b) Marov, J. N.; Reznik, E. M.; Belyaeva, V. K.; Dubrov, Y. N. *Ibid.* **1972**, *17*, 700.

(58) ^{35}Cl, $I = {}^3/_2$, 75.77 atom %, $\mu = 0.828\,13\ \beta_N$; ^{37}Cl, $I = {}^3/_2$, 24.23 atom %, $\mu = 0.684\,11\ \beta_N$.

dehyde-inhibited signal of xanthine oxidase.

This work demonstrates that the ESR line broadening (or narrowing) mechanism discussed in the context of copper(II) species[9] has considerably wider relevance and provides strong motivation for further examination of other transition metal species in the S-band range of frequencies. For example, ^{77}Se satellites from naturally abundant ^{77}Se (7.58 atom %) in $[Mo(SePh)_4]^-$ are resolved simply by lowering the frequency. Further progress in elucidating details of moderate to weak ligand hyperfine coupling would depend upon availability of techniques such as electron spin echo envelope modulation.[59,60]

(59) Mims, W. B.; Peisach, J. *Biol. Magn. Reson.* **1982**, *3*, 213.
(60) Reijirse, E. J.; van Aerle, N. A. J. M.; Keijzers, C. P.; Bottcher, R.; Kirmse, R.; Stach, J. *J. Mag. Reson.* **1986**, *67*, 114.

Successful computer simulation at more than one frequency is required for unambiguous determination of spin-Hamiltonian and line-width parameters. In the present work, this was achieved for $[Mo(abt)_3]^-$, $[MO(XPh)_4]^-$, and $[MoOL(DMF)]^+$ (L = salen, salophen), but not for $[MoO(qtl)_2Cl]$.

Acknowledgment. J.R.P. and A.G.W. acknowledge support from the Australian Research Grants Scheme. G.R.H. and G.L.W. are grateful for the award of La Trobe and Commonwealth postgraduate scholarships, respectively.

Registry No. ^{17}O, 13968-48-4; ^{77}Se, 14681-72-2; ^{35}C, 13981-72-1; ^{37}Cl, 13981-73-2; $[Mo(abt)_3]^-$, 52820-25-4; $Et_4N[MoO(SPh)_4]$, 65892-35-5; $Et_4N[MoO(SePh)_4]$, 76771-61-4; $Et_4N[WO(SPh)_4]$, 76771-66-9; $Et_4N[WO(SePh)_4]$, 76771-73-8; $[MoO(qtl)_2Cl]$, 23727-65-3; $[MoO(qtl)_Br]$, 89653-39-4; $[MoO(salen)(DMF)]^+$, 107271-65-8; $[MoO(salophen)(DMF)]^+$, 107271-66-9.

Mechanism of the Gauche Conformational Effect in 3-Halogenated 1,5-Benzodioxepins

P. Dionne and M. St-Jacques*

Contribution from the Département de Chimie, Université de Montréal, C.P. 6128, Succ. "A", Montréal, Québec, Canada H3C 3J7. *Received July 23, 1986*

Abstract: The object of this investigation is the experimental identification of the main contributing factors to the gauche conformational effect. The unique geometrical features and the flexibility of the seven-membered ring are used advantageously. The conformational changes caused by variation of the single halogen substituent at the 3-position of 1,5-benzodioxepin (**1**) are determined by quantitative dynamic NMR methods. The results show that the number of conformations varies from one to three (C_e, C_a, and TB) depending on the substituent electronegativity and solvent polarity. The trends observed for the four halogens and the methoxy group indicate that intramolecular stereoelectronic orbital interactions of the $\sigma-\sigma^*$ type are most important for the heavier halogens (I, Br, and Cl). The increasing amount of the TB form from I to Cl is a direct consequence of the increase in overlap in the $\sigma_{C-H}-\sigma^*_{C-X}$ interaction while the decreasing amount of C_e reflects on stabilization due to the $\sigma_{C-X}-\sigma^*_{C-O}$ interaction. The F substituent shows a strong departure from the trends noted for the three other halogens, while the data for the methoxy group suggest a behavior intermediate between Cl and F. For these two more electronegative substituents, the situation appears more complex as several contributing factors come into play.

Recently reported NMR studies[1,2] on the conformations of 1,5-benzodioxepins have shown that both **1** and **2** exist as mixtures of chair (C) and twist-boat (TB) conformations whereby **1** favors

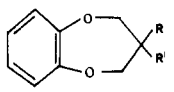

1; R = R' = H
2; R = R' = CH_3
3; R = H; R' = CH_3

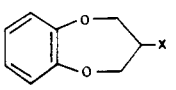

4; X = OCH_3
5; X = F
6; X = Cl
7; X = Br
8; X = I

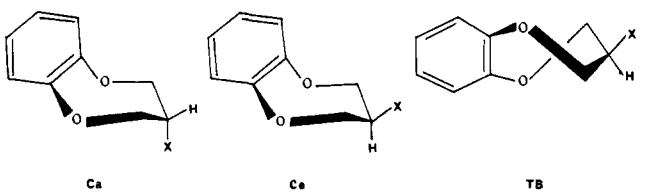

C_a C_e TB

the C form while **2** prefers the TB form. A marked difference was observed for the two monosubstituted derivatives investigated: the methyl derivative **3** exists as a mixture of three conformations, namely the chair with an equatorial methyl group (C_e), the axial chair (C_a), and the TB form, while the 3-methoxy derivative **4** reveals the presence of only two forms, C_a and TB. The latter is predominant in the polar solvent CHF_2Cl and becomes the sole conformation observed in the less polar solvent CH_3OCH_3.

These partial results have led to the present study of 3-halogenated derivatives of **1** in order to fully assess the conformational effect of single polar substituents and define the mechanism of the gauche conformational effect expected to exist in some of the conformations of these compounds. Previous reports[3-7] on this phenomenon have suggested that the underlying interactions can be either repulsive, negligible, or attractive depending on the nature of the two heteroatoms in a gauche disposition. Furthermore, recent theoretical studies[8,9] indicate that bond-antibond ($\sigma-\sigma^*$) orbital interactions in the O-C-C-X fragment are important so that the series of compounds **5-8** is expected to provide a unique molecular framework, resulting from

(1) Ménard, D.; St-Jacques, M. *J. Am. Chem. Soc.* **1984**, *106*, 2055.
(2) Ménard, D.; St-Jacques, M. *Can. J. Chem.* **1981**, *59*, 1160.
(3) Wolfe, S. *Acc. Chem. Res.* **1972**, *5*, 102.
(4) (a) Abraham, R. J.; Banks, H. D.; Eliel, E. L.; Hofer, O.; Kaloustian, M. K. *J. Am. Chem. Soc.* **1972**, *94*, 1913. (b) Kotite, N. J.; Harris, M.; Kaloustian, M. K. *J. Chem. Soc., Chem. Commun.* **1977**, 911.
(5) Zefirov, N. S.; Gurvich, L. G. *Tetrahedron* **1976**, *32*, 1211.
(6) Juaristi, E. *J. Chem. Educ.* **1979**, *56*, 438.
(7) Kirby, A. J. In *The Anomeric Effect and Related Stereoelectronic Effect at Oxygen*; Springer-Verlag: Berlin, Heidelberg, New York, 1983.
(8) Brunck, T. K.; Weinhold, F. *J. Am. Chem. Soc.* **1979**, *101*, 1700.
(9) Epiotis, N. D.; Cherry, W. R.; Shaik, S.; Yates, R. L.; Bernardi, F. *Top. Curr. Chem.* **1977**, 70.

0002-7863/87/1509-2616$01.50/0